Journal of ELECTRONIC MATERIALS, Vol. 49, No. 1, 2020
https://doi.org/10.1007/s11664-019-07753-y

Decomposed Copper(II) Acetate Over Expanded Graphite (EG) as Hybrid Filler to Fabricate Epoxy Based Thermal Interface Materials (TIMs)

SAGAR KUMAR NAYAK ,[1,2] SMITA MOHANTY,[1] and SANJAY K. NAYAK[1]

1.—SARP-Laboratory for Advanced Research in Polymeric Materials, Central Institute of Plastics Engineering and Technology, Bhubaneswar, Odisha 751024, India. 2.—e-mail: nayak.sagarkumar@yahoo.in

In this investigation, the fabrication of thermal conductive epoxy composite with the assimilation of synthesized expanded graphite (EG) decorated with copper compound nanoparticles [copper (Cu), copper(II) oxide (CuO) and copper(I) oxide (Cu_2O) nanoparticles], has been reported wherein, Cu-compound was attached to EG surface by solid-state pyrolysis of copper(II) acetate (CA) monohydrate. The prepared hybrid filler was characterized by an x-ray diffraction technique and the Cu-compound nanoparticles size was 40.8 ± 17.67 nm. The microstructure and morphology of the distributed Cu-compound nanoparticles over the EG surface were characterized by transmission electron microscopy (TEM) and scanning electron microscopy. The Cu-compound nanoparticles decorated EG hybrid filler at 10 wt.% loading ((EG-CA (4)/Ep)10) demonstrated the thermal conductivity (TC) which is 11.8 times higher than the neat epoxy due to the formation 3D percolation heat-conducting networks. Further, decoration of Cu-compound on the EG surface resulted in higher TC as measured using a guarded heat flow meter technique. Lap shear strength of (EG-CA (4)/Ep)10 composite was tuned to 5.93 ± 0.27 MPa as characterized by a universal testing machine. The porosity of fabricated composites was decreased as Cu-compound attachment increases on the EG substrate. The thermo-gravimetric analysis revealed enhanced thermal stability of (EG-CA (4)/Ep)10 composite to 407°C at 50% weight loss consideration. The electrical resistivity of the composite was reduced with the addition of the EG filler system as confirmed from the super megaohmmeter.

Key words: Hybrid composites, thermal conductivity (TC), expanded graphite (EG), copper compound nanoparticles, epoxy matrix

INTRODUCTION

The polymeric materials have unique characteristics like lightweight, low cost, easy processability, and electrical insulation, which satisfy the requirement to fabricate the electronics packaging materials.[1–3] Due to the rapid development of more miniaturized, lighter, multifunctional and high power density microelectronics circuits, heat production increases which can affect the performance, reliability and lifetime of electronic devices. Thus, the heat removal from source to sink becomes the crucial issue as multifunctional efficient circuits are the industry demand. For this, thermal conducting and electrical insulating or semiconducting

(Received May 15, 2019; accepted October 18, 2019; published online November 1, 2019)

polymer-based thermal interface materials (TIMs) are in high demand.[4–6] However, most of the polymer has undesired TC below 0.6 W/mK, which is incapable to meet the requirement of thermal management in the highly-efficient electronic devices.[7]

Out of different types of polymeric materials, epoxy resin is used in electronics and electrical appliances for its outstanding physical and chemical properties. Thus, epoxy resin is high-performance thermosetting resin attributing high mechanical and adhesive properties, excellent dimensional and thermal stability, fine electrical insulation, low outlay, and better processing ability, etc. However, low TC (0.19 W/mK) of epoxy resin restricts the application as heat-dissipating packaging materials.[8,9] To cope with thermal management issue, the most economical and prominent way is to improve the TC of epoxy resin with the incorporation of ultra-high thermal conducting fillers. The typical thermal conducting fillers such as carbon filler (graphite, expanded graphite (EG), graphene and CNT),[10–12] ceramic fillers [aluminum oxide (Al_2O_3), boron nitride (BN), aluminium nitride (AlN) and beryllium oxide (BeO)],[13,14] and metallic filler [silver (Ag), copper (Cu), Aluminum (Al) etc.][15,16] are usually incorporated in an epoxy matrix by melt mixing and/or solution mixing. To obtain the desired TC limit of epoxy composite, the ceramic and metallic filler is incorporated at large weight % due to high weight density of fillers. Such high filler fraction (> 60 wt.%) diminishes the mechanical properties of the composite which hinders the prospective application in the final stage. This drawback has been overcome by the addition of 3-D low-density graphitic foam such as EG which was synthesized in an economical way in this work.

To prepare the EG-Cu-compound hybrid filler, a simple technique of 'mix and heat' was followed.[17] The weakly bonded hexagonal layers in EG are separated by a few nanometers leads to a high aspect ratio (200–1500) and high modulus of elasticity (~ 1TPa).[18] Previously EG was prepared by adopting a sophisticated and risky technique in which a large amount of concentrated H_2SO_4 and HNO_3 was utilized. In this work, the EG was synthesized from natural graphite flake (NGF) through a simple and scalable two-step method with intercalation of ammonium persulfate ($(NH_4)_2S_2O_8$) and 85% less quantity of concentrated H_2SO_4.[19] Moreover, EG possesses excellent thermal and electrical conductivity along with high thermal stability and mechanical strength. When compared to other carbon derivative materials (graphene oxide, graphene), EG preserves simple and cost-effective production process which is ascribed to the economical development of different polymer composites.[20,21]

Due to the high aspect ratio, surface area and strong interactions towards metal particles, the Cu-compound nanoparticle can easily disperse on the surface of EG.[22,23] The thermal decomposition of CA in the air at 300°C gives rise to the mixture of Cu, CuO and Cu_2O.[24] From the solid-state reduction of CA, many experimental outcomes were obtained. Afzal et al.[25] yielded Cu, CH_3COOH, CO_2, C, and H_2 after dehydration of anhydrous CA. Mansour et al.[26] demonstrated CA decomposition in two steps. The initial dehydration was at 190°C followed by partial decomposition at 220°C. The outcomes were CuO with the traces of Cu_2O and Cu_4O_3. Zhang et al.[27] also indicated CA decomposition in four stages in air ascribing two initial reversible steps and the last two irreversible steps. Although the above analysis on the CA decomposition contradicts each other, we decomposed CA monohydrates on the EG surface to get hybrids of the EG-Cu-compound.[28] Yan et al.[29] prepared a hybrid of reduced graphene oxide (r-GO)/cuprous oxide (Cu_2O) nanoparticles from oxygen reduction reaction using diethyl glycol as a reducing agent and solvent. This hybrid is used as an anode material in lithium-ion batteries and, the catalyst for degradation of dye. d'Halluin et al.[30] fabricated graphite- supported Cu nanoparticles by the reduction of CA with H_2.

Lifeichen et al.[31] synthesized silver-graphene nanosheets (GNSs) hybrid filler by mixing and heating of GNSs and silver acetate salt and fabricated in epoxy-based TIMs. At 1.5 mol.% of Ag nanoparticles on the GNS, the TC of epoxy composite enhanced to 280% as compared to neat epoxy. Liu et al.[32] studied the comprehensive application of MWCNT, Cu and CuO nanoparticles in ethyl glycol, engine oil, and water as a matrix to prepare thermal conductive nanofluid. They demonstrated that the TC improvement of CuO and MWCNT nanofluid is approximately linear. Hence, the effect of Cu, CuO and Cu_2O nanoparticles in the epoxy matrix is obvious and, hence, the EG surface coated Cu-compound nanoparticles will establish a new insight of TC enhancement of epoxy hybrid composite.[17]

In this work, the TC of the fabricated hybrid composites is based on the compatibility of tri filler systems such as carbon (EG), metallic (Cu) and ceramic (CuO and Cu_2O). So Mun et al.,[33] encapsulated the EG surface with two different ceramic materials, i.e., BN and SiO_2 and achieved a higher TC value of 3.3 W/mK at 10 wt.% loading of BN/SiO_2/EG hybrid filler, whereas only EG/epoxy composite demonstrated ~ 5.5 W/mK of TC value. To reduce Kapitza resistance the at filler-matrix interface, high-temperature application is indispensable which results in high TC value for composites containing hybrid of micro and nanofiller.[31,34]

EXPERIMENTAL

Materials

The natural graphite flakes (NGF) of size ~ 200 μm were supplied by Sigma Aldrich, USA. Sulfuric acid (98%) was from Avra synthesis Pvt. Ltd., Hyderabad, India. Ammonium persulfate was

supplied by Merek life science Pvt. Ltd. Mumbai, India. Copper(II) acetate (98%) monohydrate was procured from Sigma Aldrich, India. DGEBA epoxy resin (Araldite GY 250) and low viscous cross-linking agent tri-ethylene tetraamine (TETA) were supplied by M/S Huntsman International Pvt. Ltd. India.

Synthesis of EG and EG-Cu-Compound

The two-step preparation of EG has been presented in Fig. 1. First the slurry of $(NH_4)_2S_2O_8$ and conc. H_2SO_4 was mixed with a composition of 5 g and 3 mL, respectively, followed by 10 min sonication. Then 1 g of NGF was added to the slurry for 1 min agitation at room temperature. Within 24 h, the reaction was converted into the worm and cauliflower-like appearance called intercalated graphite compound (IGC). The acid content in the IGC was washed with distilled water and drained water was observed by litmus paper. Further acid-free IGC was dried in a vacuum oven at 100°C for 24 h. In the second step, to get more expandable structure and volume, the IGC was kept at 860°C for 90 s inside the muffle furnace. Due to the high thermal shock, the sudden evaporation of the intercalated compound breaks the Van der Waals force in the graphitic basal plane that leads to the formation of EG.

Then copper(II) acetate (CA) or cupric acetate which appears as a dark green crystalline solid was mixed with EG with a different weight ratio. In the first proportionate, EG and CA powder with the ratio of 5:2 were mixed with a cryo mill at 20 Hz frequency. Similarly, the next proportionate with a ratio of 5:4 was prepared. Then following the 'mixed and heat' techniques,[31] the absence of any solvent, reducing agent or electric current, the mixture was heated at decomposition temperature of acetate (~ 300°C) in an ambient atmosphere for 20 min

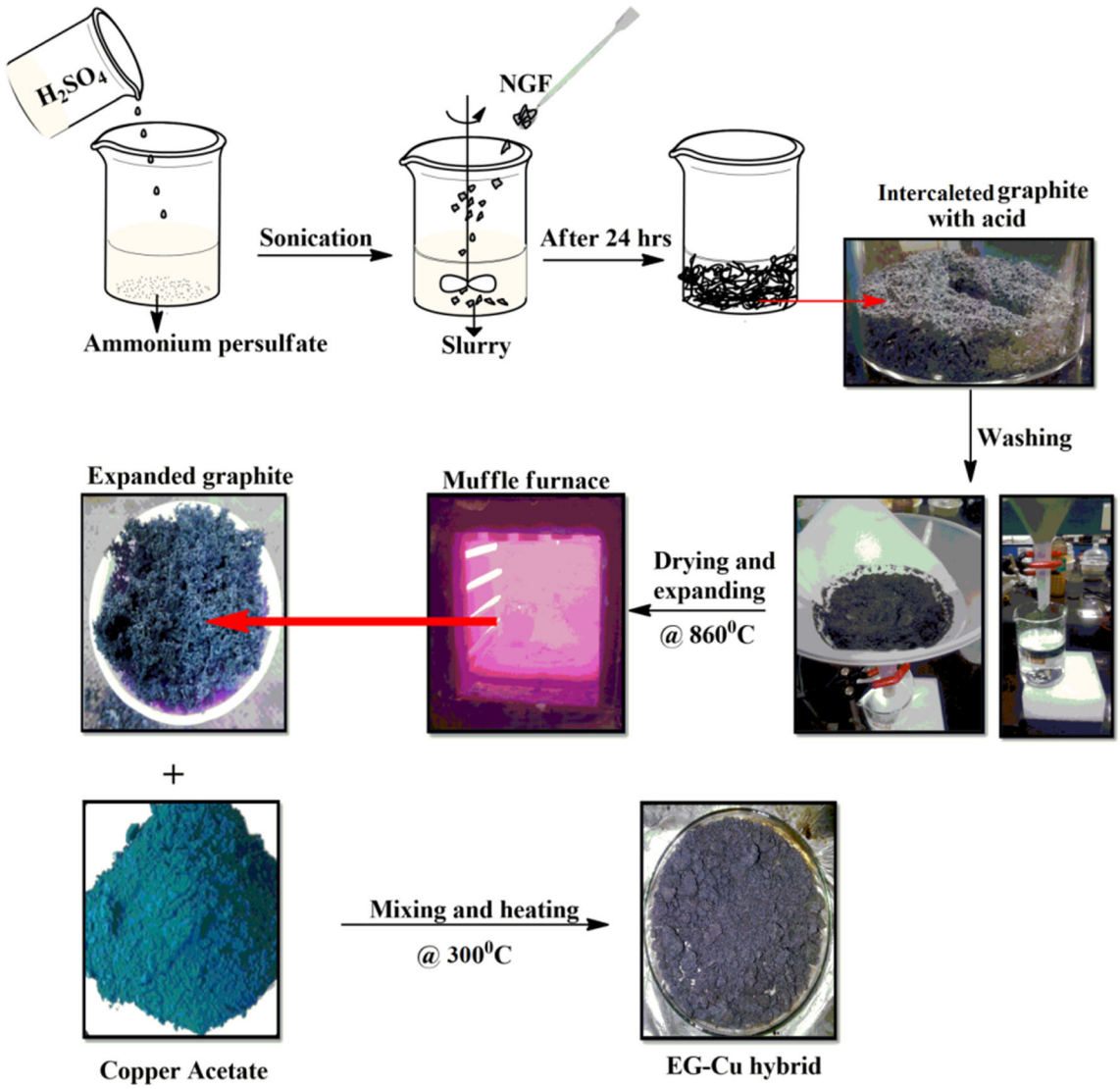

Fig. 1. Preparation method of EG-Cu compound hybrid filler.

(Fig. 1). The CA, after 20 min, was converted into corresponding metal and metal oxide and formed nanoparticles on the surface of EG.

Fabrication of Thermally Conductive Composite

The EG-Cu compound epoxy hybrid composites were fabricated following stir-casting techniques. A certain amount (i.e., 2.5 wt.%, 5 wt.% and 10 wt.%) of synthesized EG-Cu compound hybrid fillers was dried in a vacuum oven at 60°C. At the same time, epoxy resin and hardener (HY950) were selected in the ratio of 10:1 and epoxy resin was kept in a vacuum oven at 70°C for 1 h to reduce viscosity. The predefined amount of dried EG-Cu-compound hybrid filler was added to low viscous epoxy resin summarized in Table I, followed by 1 h mechanical stirring. Then the uncured composite kept in ultrasonication bath for 2 h to ensure uniform distribution of hybrid filler in the matrix. Then hardener was mixed gently followed by few min sonications and degassing through a vacuum pump. The prepared EG-Cu-compound hybrid composites were poured into the mould and left for 24 h with the 5 kg load applied to make a compact composite. Then solid composites were demoulded for further specimen cutting as these have to pass through various characterization techniques.

Characterization

Use of a laser diffraction particle size analyzer (LA-960, Horiba Scientific) was carried out to measure the particle size of CA suspension as per the dynamic light scattering (DLS) technique. The crystal structure and morphology of EG and EG-Cu-compound hybrid filler were characterized by x-ray diffraction (XRD) technique (Shiadzu, XRD-7000L, Japan). The source of the x-ray is Cu-Kα radiation. The morphology of EG-Cu-compound hybrid filler was characterized by scanning electron microscopy (SEM, Carl Zeiss SMT Germany) and transmission electron microscopy (TEM, JEM-2100). The through-plane TC of the composite system was measured at 90°C through a guarded heat flow meter technique as per ASTM E 1530-06 (Unitherm 2022, Antercorpo, USA). The instrument is based on Eq. 1

$$Q = KA\left[\frac{T_1 - T_2}{L}\right], \tag{1}$$

where Q is the heat flux through-plane (Watt); K is the steady-state thermal conductivity of composite (W/mK); L is the plane thickness (m) and A is the plane area (m^2). The dimension of the composite sample is with a 50 mm diameter and 4 mm thickness. The single-lap shear strength of each hybrid sample was pulled out by the universal testing machine (UTM, Instron 3382, UK) at a crosshead speed of 0.05 inch/min as per ASTM D1002. Two mechanically polished (by 400-grade emery paper) aluminum sheets were stuck together using prepared composite adhesive with bond line thickness (BLT) of 0.05–0.1 μm as described in Fig. 2.

The rotating spindle viscometer (Brookfield, DV-II + Pro) was used to analyze shear viscosity. The shear viscosity of uncured epoxy composite is determined from the shear rate which depends on rotational speed, tool geometry, and size of the sample container. The thermal stability of hybrid composites was carried out by thermogravimetric analyzer (TGA, TA Instruments, USA) using indium as the reference material according to ASTM E1868. The TGA analysis was carried out by taking the sample in the pan (5–10 mg) and the temperature was increased by 10°C/min over a temperature range 30–600°C under nitrogen purging with a flow rate of 60 mL/min. The electrical resistivity of hybrid composites was evaluated by a super mega ohmmeter, SM-8220 (M/s TOA electronics Ltd. Japan) as per ASTM D257. A round disc of 100 mm diameter and 3 mm thickness was fabricated for testing. The fracture surfaces of the optimized hybrid composites system were examined using SEM at different magnification.

RESULTS AND DISCUSSION

CA hydrate demonstrates the paddlewheel structure having a density of 1.88 g/cm^3. The particle size distribution of CA is shown in Fig. 3. DLS technique

Table I. Composition of the fabricated epoxy composite system

Sl. no.	EG-CA ratio	EG-Cu compound (wt.%)	DGEBA (wt.%)	Sample code
1	–	2.5 (neat EG)	97.5	(EG-CA (0)/Ep)2.5
2	5:2	2.5	97.5	(EG-CA (2)/Ep)2.5
3	5:4	2.5	97.5	(EG-CA (4)/Ep)2.5
4	–	5 (neat EG)	95	(EG-CA (0)/Ep)5
5	5:2	5	95	(EG-CA (2)/Ep)5
6	5:4	5	95	(EG-CA (4)/Ep)5
7	–	10(neat EG)	90	(EG-CA (0)/Ep)10
8	5:2	10	90	(EG-CA (2)/Ep)10
9	5:4	10	90	(EG-CA (4)/Ep)10

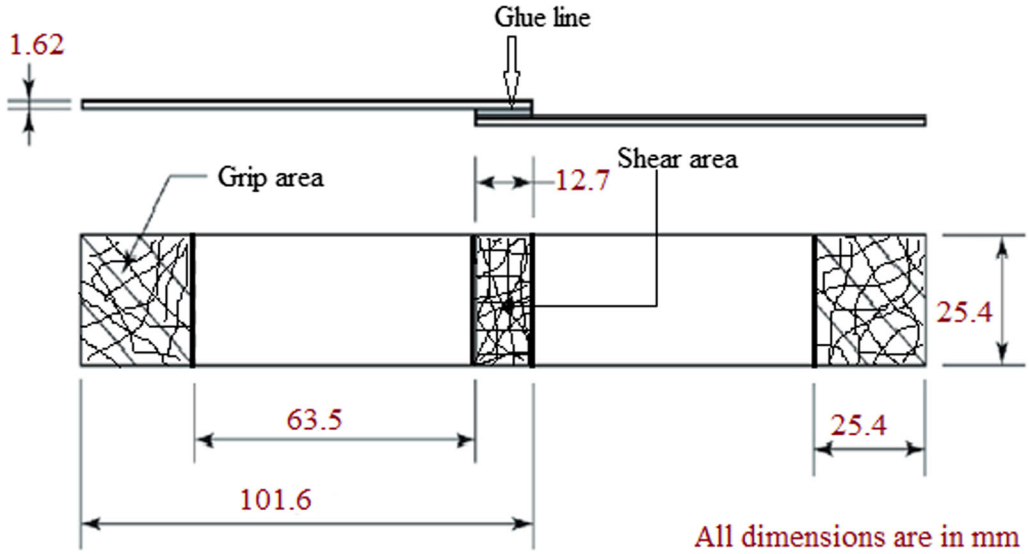

Fig. 2. Schematic diagram of the epoxy-based single lap joint of aluminum substrates.

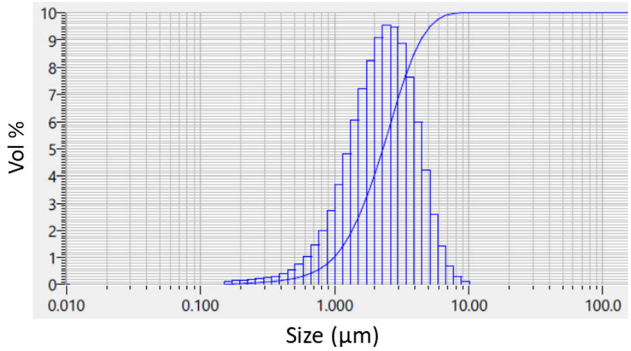

Fig. 3. DLS results of CA water suspension.

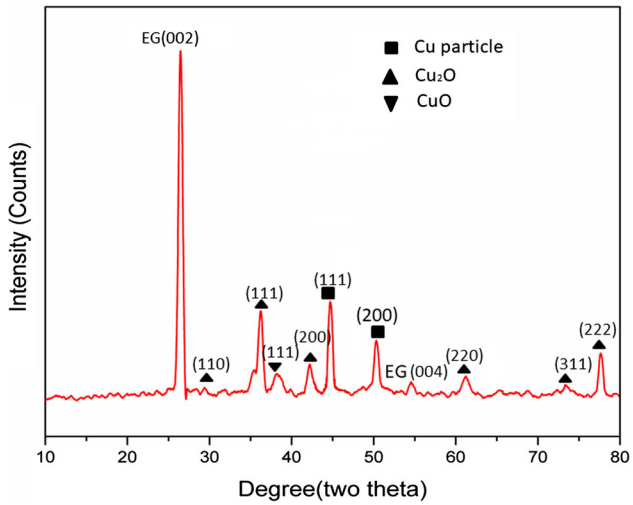

Fig. 4. XRD pattern of EG-Cu-compound hybrid filler.

indicated the average particle size of CA is 2.5 μm with a standard deviation of 1.39.

Figure 4 illustrates the XRD patterns of EG-Cu-compound hybrid filler (EG:CA::5:2). The crystalline nature of EG was quite visible from intense peaks at 2θ = 26.58° and 2θ = 54.91°, corresponding to (0 0 2) and (0 0 4) diffraction, respectively.[35] This may be due to the presence of H_2SO_4 and $(NH_4)_2S_2O_8$ in a certain proportionate and immediate hold on of intercalated graphite compound at a high temperature which exhibited chemical oxidation that leads to an expansion of graphite basal plane.[36] As per Bragg's equation ($n\lambda = 2d\sin\theta$), the interlayer distance (d) between two layers of EG is 0.335 nm at x-ray wavelength λ = 0.154 nm. A week diffraction peak at 2θ = 54.91° may be due to the incomplete oxidation. The peaks at (1 1 1) and (2 0 0) are observed from the XRD diffractogram at a diffraction angle of 44.22°, and 50.1°, respectively, as per face-centered cubic (FCC) analysis of copper metal (JCPDS Copper: 04-0836). The diffraction peaks (110), (111), (200), (220), (311), and (222) are observed at the diffraction angles of 30°, 36.3°, 42.1°, 60.7°, 73.32°, 77.5°, respectively due to the formation of Cu_2O (JCPDS 78-2076). The broad diffraction peak (111) is detected at a diffraction angle of 38.2° is due to the traces of CuO.[24,29] The mean size of the Cu-compound particle has been estimated by Scherer's equation (Eq. 2).

$$d = \frac{0.9\lambda}{\beta \cos\theta}, \tag{2}$$

where d = mean diameter of the copper particle and β = angular Full width half maximum (FWHM) in radians. From the XRD data, the mean diameter of the Cu and Cu-oxide particle was estimated as 40.8 ± 17.67 nm at different diffraction angles mentioned in Fig. 4 which is also, confirmed from the TEM image (Fig. 5).[37] From Fig. 5a and b, the Cu and Cu-oxide (s) nanoparticles are quite visible. There were no CA diffraction patterns appearing in the XRD graph of the final hybrid filler, which

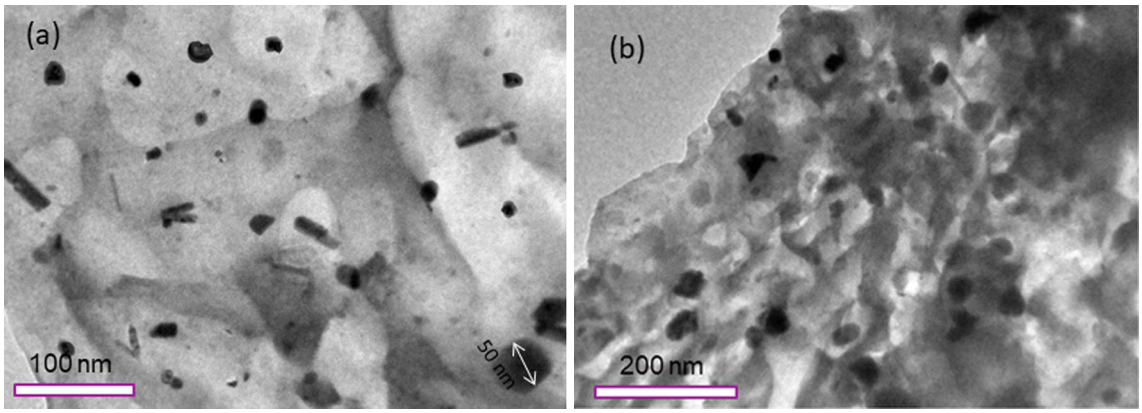

Fig. 5. TEM images of 2 wt.% CA loading to EG (a) and (b).

suggested that the salt-to-metal and salt-to-metal oxide (s) conversion was almost completed.

Figure 6a and b reveal the expansion of the graphitic layers in EG which is the combination of numerous GNSs (< 100 nm) with micro dia (< 10 μm). The interconnected lamellar and loose structure of EG signifies that the petite amount with the epoxy matrix can enhance the thermal properties effectively. The Cu and Cu-oxide (s) nanoparticles are attached to EG substrates and distributed uniformly as illustrated in Fig. 6c and d. The growth of nanoparticles on the substrate of EG making few clusters is also noticed and, hence, attachment of substrate-particle and particle-particles is the evidence of hybrid filler formation. Due to the high surface area to volume of Cu and Cu- oxide nanoparticles, the agglomeration of particles has been observed in Fig. 6e and f. It may be that the increasing of CA loading from a ratio of 2–4 with EG, causes the size of nanoparticles to also grow.[17,31]

In Lin's study,[17] the thermal decomposition of metal acetate typically yields the corresponding metal or metal oxide which is similar to the conversion of metal nitrate that has been documented. The gold(III) acetate, cobalt(II) acetate, nickel(II) acetate and palladium(II) acetate decomposed to the respective metal nanoparticles on substrates like carbon (EG, CNT, CNF, etc.) and ceramic particles (Zeeosphere, silica-alumina microsphere, etc.). However, iron(II) and zinc(II) acetate yielded nanohybrids of corresponding metal oxide nanoparticles. They reported that on MWCNT substrates, the lead(II) acetate decomposed to metallic lead (Pb) and lead oxide (PbO). Moreover, copper(II) acetate disintegrated into metallic copper (Cu) on the MWCNT surface. However, in our study, in the presence of monohydrates, the copper(II) acetate yielded nanohybrids of Cu, CuO, and Cu_2O as evidenced by XRD analysis (Fig. 4).

The through-plane TC improvement of epoxy composite by integrating EG and EG-Cu- compound hybrid filler is depicted in Fig. 7a, b and c. Table II summarizes the TC and TR of the composite sample including enhancement (%) as compared to neat epoxy. The composite coded as (EG-CA (0)/Ep)2.5, (EG-CA (0)/Ep)5, and (EG-CA (0)/Ep)10, contained 2.5 wt.%, 5 wt.% and 10 wt.% of synthesized EG, respectively, and accordingly the TC of the corresponding composites improved by the factor of 1.62, 5.04 and 8.7 with respect to neat epoxy, respectively. This TC enhancement of the epoxy composite is due to the high TC value of EG ($\sim$ 100 W/mK), whichis attributed to the obvious enhancement of TC of epoxy composite by forming a phonon transfer linkage inside the epoxy matrix.[33]

Figure 7a illustrates the 2.5 wt.% incorporation of neat EG and EG-Cu-compound hybrid. The composite coded as (EG-CA (2)/Ep)2.5 contained 2.5 wt.% of EG-Cu-compound hybrid filler (5:2) showing the TC of 0.92 times higher than neat EG loaded composite. Similarly, the (EG-CA (4)/Ep)5 named hybrid composite carried 2.5 wt.% of EG-Cu-compound hybrid filler (5:4) demonstrates the TC of 1.23 times as compared to (EG-CA (2)/Ep)2.5 hybrid composite. From Fig. 7a, it is also observed that, as the TC of the above-described hybrid composite increased, the equivalent TR (TR of the unit area of the material) is decreased. Low TC value induces high insulation of the materials in thermal contact. The TR of lowest TC valued neat epoxy is 20.72×10^{-3} m^2K/W, and it suddenly diminished to 11.82×10^{-3} m^2K/W after 2.5 wt.% of neat EG addition. Then this TR value abruptly reduced when EG-Cu-compound hybrid filler at equal wt.% incorporated to epoxy resin. From the above analysis, it can be concluded that epoxy resin-based TIMs with EG-Cu compound hybrid filler is encouraging better phonon transport than neat EG loaded epoxy composites. The Cu and CuO nanoparticles possess the TC of $\sim$ 400 W/mK and $\sim$ 33 W/mK, respectively, which contributed to the TC enhancement in the hybrid epoxy composite. The synergistic coalition of the EG and Cu-compound nanoparticles reduced the phonon scattering at the interface of filer and matrix.[32] A similar improvement of TC has been

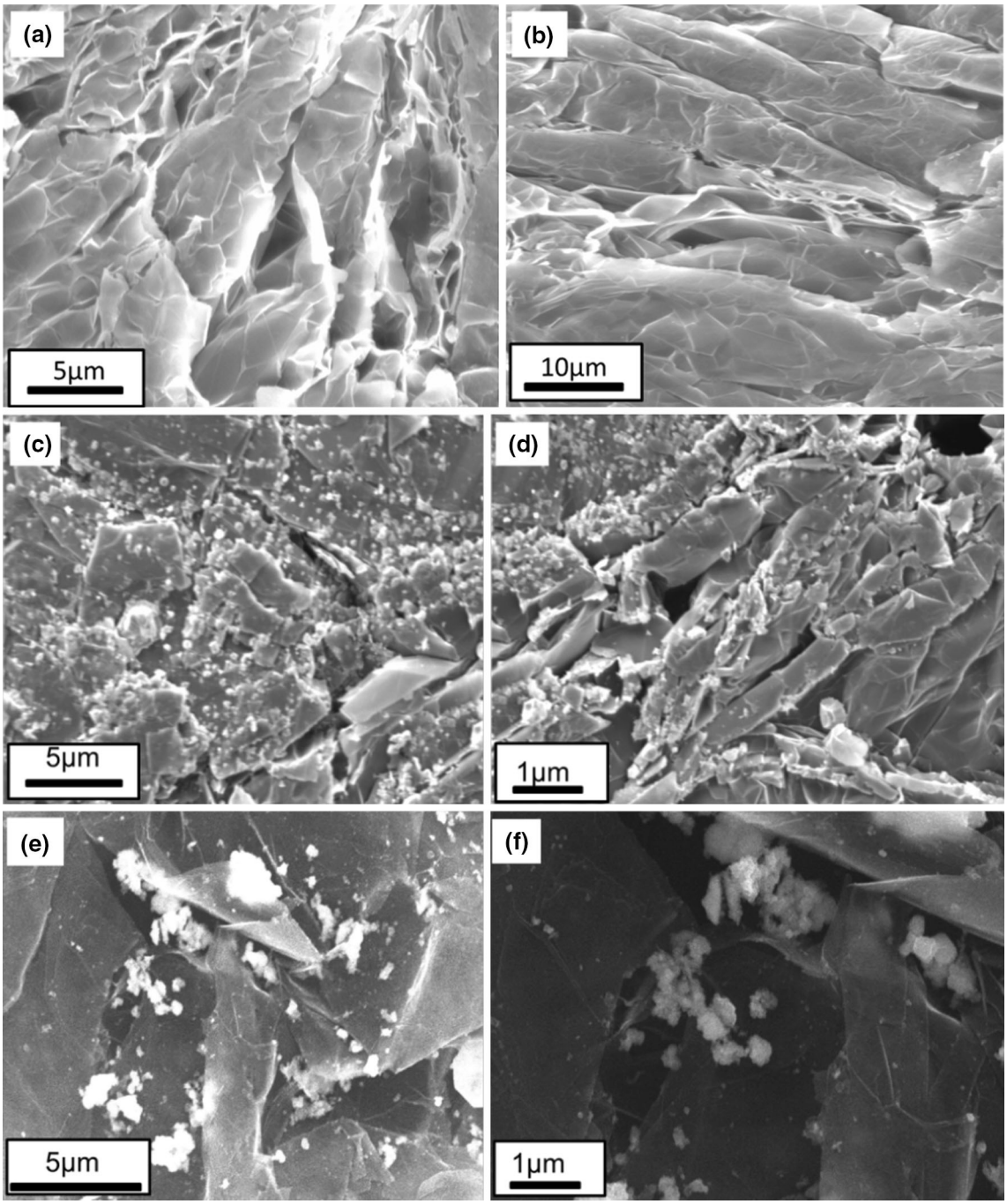

Fig. 6. (a) and (b) SEM images of EG, (c) and (d) CA mixing with EG in the ratio of 2:5, (e) and (f) CA mixing with EG in the ratio of 4:5.

observed at 5 wt.% of EG-Cu-compound hybrid filler. The hybrid composite entitled (EG-CA (0)/Ep)5 (5 wt.% near EG) is showing five times enhanced TC value as compared to neat epoxy. This is due to the higher filler loading of EG that enables the conductive network formation through which phonon transfer takes place. With the same (5 wt.%) filler fraction addition of EG-Cu compound hybrid filler comprising the hybrid composites named as (EG-CA (2)/Ep)5 and (EG-CA (4)/Ep)5 are displaying a resultant TC value of 5.24 and 6.65 fold higher than neat epoxy (Fig. 7b). The TR of above mentioned two-hybrid composites takes a sharp fall to 3.12×10^{-3} m^2 K/W at 5 wt.% addition of EG-Cu compound hybrid filler.

The TC of three optimized composites carrying 10 wt.% of neat EG and EG-Cu-compound hybrid filler depicted in Fig. 7c. At 10 wt.% loading of EG-Cu-compound hybrid filler, the composite coded as (EG-CA (2)/Ep)10 and (EG-CA (4)/Ep)10 demonstrated the TC enhancement of 9.68 and 11.81 fold as compared to neat epoxy. The (EG-CA (4)/Ep)10

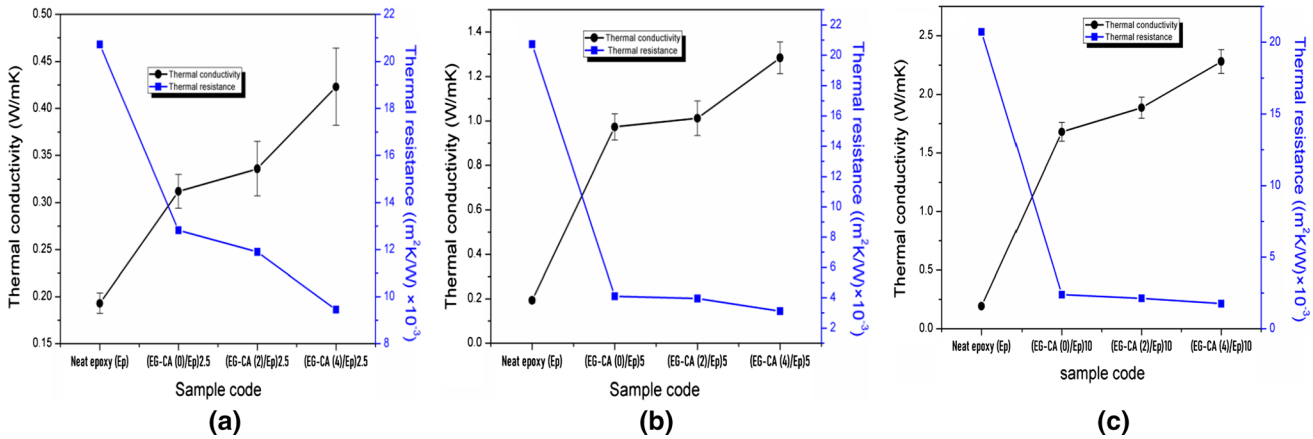

Fig. 7. Thermal conductivity (TC) and thermal resistance (TR) of EG-Cu compound hybrid epoxy composite system at (a) 2.5 (b) 5 and (c) 10 wt.% filler addition.

Table II. Thermal Conductivity (TC), thermal resistance (TR) and enhancement (%) of EG-Cu compound hybrid composite system

Sample code	Thermal conductivity (W/mK)	Enhancement (%) $\frac{K-K_0}{K_0}$	Equivalent thermal resistance (m^2 K/W) × 10^{-3}
Neat epoxy (Ep)	0.193 (K_0)	–	20.72
(EG-CA (0)/Ep)2.5	0.312	61.65	12.82
(EG-CA (2)/Ep)2.5	0.336	74.09	11.9
(EG-CA (4)/Ep)2.5	**0.423**	119.17	9.45
(EG-CA (0)/Ep)5	0.973	404.14	4.11
(EG-CA (2)/Ep)5	1.012	424.35	3.95
(EG-CA (4)/Ep)5	**1.284**	565.28	3.12
(EG-CA (0)/Ep)10	1.679	769.95	2.38
(EG-CA (2)/Ep)10	1.886	877.2	2.12
(EG-CA (4)/Ep)10	**2.28**	1081.34	1.754

Bold values indicate highest TC result of corresponding composite system.

named hybrid composite showed the highest TC of 2.28 W/mK and lowest TR of 1.75 × 10^{-3} m^2 K/W among all the fabricated composite. The combined effect of Cu, CuO, and Cu_2O nanoparticles with EG at minimum weight fraction appendage a new insight towards TC enrichment of epoxy-based TIMs. The Cu and Cu-oxides(s) nanoparticles act as spacer between EG strands which build bridges for phonon transport paths.[38,39] As the CA mixing ratio proliferates from the ratio of 2–4 on the EG surface, the mean size decomposed of Cu and Cu-oxide (s) also grows to two to three times. Thus, the large particle size minimized the phonon-scattering and reduces the acoustic impendence mismatch in the epoxy composite.[40] The combining effect of fillers with different sizes from nm to μm and μm to mm is beneficial for TC enhancement through the heat-conducting paths and distribution intensity of the filler in the matrix.[41] The above analysis corroborated the contribution of EG-Cu-compound hybrid filler for TC enhancement of hybrid epoxy composite.

Wang et al.[21] fabricated a silane-modified EG/epoxy composite at 4.5 wt.% loading that shows the TC value of 1.0 W/mK which is 28.4% lower than our work (5 wt.% loading of EG-Cu-compound). Kumar et al.[42] achieved the TC of 3 W/mK of the epoxy adhesive by optimizing 40 wt.% of EG/GNP hybrid. However, due to higher filler loading, the lap shear strength reduced significantly. Goyal et al.[43] fabricated hybrid graphene-metal epoxy composite by dispersing the graphene in the electrically conductive silver epoxy. By 5 vol.% graphene incorporation; the TC of the resulted hybrid composite was increased by ~ 500% between the temperature ranges of 300 K to 400 K and Cu_2O nanoparticles in the epoxy matrix are obvious.

Apart from epoxy, polydimethylsiloxane (PDMS) with lower compressive modulus than epoxy is also suitable matrix material to fix the challenges as electronics packaging materials. Pettes et al.[44] prepared nickel foam templated graphene framework by CVD which was added to PDMS by Fang et al.[45] Fang et al. reported that at 11.6 wt.% densely packed graphene framework addition to PDMS matrix showed through-plane TC of 1.62 W/mK. Similarly, in another work of Fang et al.,[46] the incorporation of 33.8 wt.% of dense graphene foam

and h-BN to PDMS matrix gave rise to the composite TC of 2.11 W/mK. Kim et al.[47] collected five types of GNP (IC500, M5, M15, M25, H5) and prepared the GNP/polycarbonate composite using a typical melt mixing process. The TC was enhanced to 121% as per the filler lateral size. The highest through-plane TC at 20 wt.% GNP addition was 1.8 W/mK. Haeejal Jung et al.[48] oriented graphene nanoflakes (GNF) in an L shaped kinked tube containing PVDF (polyvinyl difluoride) matrix through solution casting using the melt-compression method. The PVDF/GNF composite at 25 vol% of GNF in melt-flow direction gave rise to the directional TC of 10 W/mK. They mentioned that this method of polymer composite preparation attributed better results as compared to CNT, 3D-graphite filler (EG) loaded epoxy composite.

Adhesive bond strength is typically evaluated by a lap shear test where test specimen is subjected to a tensile pull tangentially. The failure stress is basically measured by dividing the failing load by adhesive bond area.[49] The tensile single lap shear strength (LSS) of the adhesive joints of neat epoxy, as well as the six different adhesive composites, are depicted in Fig. 8. The results are summarized as per scattering results through standard deviation (Table II). It is observed that LSS of neat epoxy is 4.41 MPa and with 5 wt.% addition of EG, the improvement is about 7.7% with respect to neat epoxy. The increment of the cohesive strength of prepared composite and interfacial bond strength between the substrate and composite adhesive attributed the LSS improvement.[42,50] The significant changes have been noticed for sample (EG-CA (4)/Ep)5, in which the LSS enhanced to 6.13 MPa which is 39% higher than LSS of neat epoxy. The enhancement can be ascribed by the presence of Cu and Cu oxide(s) nanoparticles which nurture good adhesion between epoxy resin and filler as nanoparticles exhibit high surface area to volume ratio. As EG retains a high aspect ratio along with carboxylic (–COOH) and hydroxyl (–OH) functional groups and Cu oxide(s) exhibits oxygen functionality, they are liable to interact with surrounding epoxy and TETA and supplemented the LSS of the hybrid epoxy composite system.[21,42]

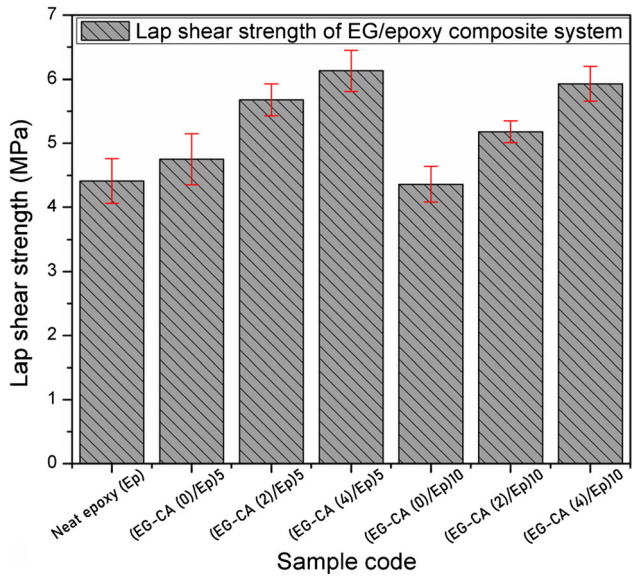

Fig. 8. Lap shear strength of hybrid epoxy composites system.

From Fig. 8, it is evident that the values of LSS of the composite containing 10 wt.% of EG ((EG-CA (0)/Ep)10) is slightly reduced with respect to neat epoxy. The porous and layered architecture of EG responsible for this reduction. The uniform mixing of EG throughout the epoxy matrix becomes a little tough at higher filler loading which creates some micro gaps and void throughout the composite system.[51] Also, the reduction in LSS can be attributed to the crowding effect of filler that can accelerate crack initiation and propagation in the composite system.[52] A similar agglomeration effect has been observed in our previous research.[1,42,50] Furthermore, the addition of hybrid filler of EG-Cu-compound at equivalent wt.%, the LSS of hybrid composites such as (EG-CA (2)/Ep)10 and (EG-CA (4)/Ep)10 enhanced to 19% and 36% with respect to bare EG loaded epoxy composite, respectively. This happens due to the high-frequency mixing of EG and CA and then heating of mixed filler leads to better symmetry among themselves. Also, the coated nanoparticles and functional groups bind the epoxy material (DGEBA and TETA) affirmatively.[52] This is also described so that the Cu-compound nanoparticles can create bridges linking the EG strand in the epoxy resin with better dispersion. Thus, the cohesive strength of epoxy adhesive

Table III. The lap shear strength, modulus, and types of joint failure of the epoxy composite system

Sample code	Shear strength (MPa)	Elongation at break (%)	Modulus (MPa)	Mode of joint Failure
Neat epoxy (Ep)	4.41 ± 0.35	0.42 ± 0.01	1049.08 ± 58.37	Interfacial
(EG-CA (0)/Ep)5	4.75 ± 0.4	0.51 ± 0.03	930.64 ± 23.75	Partially cohesive
(EG-CA (2)/Ep)5	5.68 ± 0.25	0.56 ± 0.03	1014.63 ± 9.73	Partially cohesive
(EG-CA (4)/Ep)5	6.13 ± 0.32	0.6 ± 0.02	1021.23 ± 19.3	Fully cohesive
(EG-CA (0)/Ep)10	4.36 ± 0.28	0.48 ± 0.01	927.8 ± 52.8	Fully cohesive
(EG-CA (2)/Ep)10	5.18 ± 0.17	0.52 ± 0.05	1000.82 ± 62.93	Partially cohesive
(EG-CA (4)/Ep)10	5.93 ± 0.27	0.53 ± 0.02	1118.64 ± 8.73	Partially cohesive

Table IV. Theoretical and experimental bulk density of the epoxy composite system

Sl. no.	Sample code	Filler volume fraction	Theoretical density (g/cc)	Experimental density (g/cc)	Porosity/void content (%)
1	(EG-CA (0)/Ep)5	0.63	0.42	0.39 ± 0.02	7.14
2	(EG-CA (2)/Ep)5	0.6	0.45	0.426 ± 0.014	5.33
3	(EG-CA (4)/Ep)5	0.59	0.46	0.448 ± 0.011	2.6
4	(EG-CA (0)/Ep)10	0.78	0.26	0.219 ± 0.018	15.76
5	(EG-CA (2)/Ep)10	0.77	0.28	0.253 ± 0.016	9.64
6	(EG-CA (4)/Ep)10	0.75	0.29	0.278 ± 0.01	4.13

hybrid composites is enhanced progressively with the same wt.% (10 wt.%) of hybrid filler addition.

It is also worth mentioning that the lap shear properties of an adhesive joint essentially depend on bond line thickness (BLT) of adhesives and surface treatment of the aluminum substrate which is a crucial factor for interfacial bond strength. Ghosh et al.[49] reported that surface treatment of aluminium sheets such as mechanical polishing results in better joint strength with epoxy adhesive due to the formation of oxygen-deficient aluminium oxide (Al_2O_3). This can be ascribed to that the electron sharing between oxygen present in epoxide dimer and trimer of adhesive and oxygen-deficient substrates leading to stronger bonding between adhesive and substrates which established improved joint strength.[49] Since the surface treatment to establish good interfacial bond strength for all epoxy composites is pragmatically the same, then the factor, cohesive property distinguishes and becomes a decisive factor for the LSS of different composites, loaded with different type filler. The mode of failure of the hybrid epoxy composite is summarized in Table III including modulus of elasticity. It is observed that cohesive strength (adhesive–adhesive) is predominant over interfacial adhesive strength (adhesive- substrate). Hence, the adhesive failure mode demonstrated comparatively higher LSS value. The increase in LSS of the hybrid epoxy composite happened mostly due to the resistance to fracture provided by the hybrid filler with the help of a crack-blunting mechanism.[53,54] From earlier observation, it is confirmed that the relative decrease in LSS with an increase in filler loading to 15% may be due to the formation of fault-containing aggregations of fillers and stress concentration around the filler inside the epoxy matrix.[55]

Table IV summarizes the bulk density and porosity of the hybrid epoxy composite containing different weight fractions of EG-Cu compound hybrid filler. The theoretical bulk density of the composite system in terms of weight fraction can be obtained by the Agarwal and Broutman equation (Eq. 3)

$$\frac{1}{\rho_{ct}} = \frac{w_f}{\rho_f} + \frac{w_m}{\rho_m}, \tag{3}$$

where, w and ρ signify the weight fraction and density, respectively. The suffix f, m, and ct stand for the fiber, matrix, and composite, respectively. The actual density (ρ_{cm}) of the composite, however, can be determined manually by a simple water immersion method. The void content or porosity of the composites is calculated using Eq. 4.

$$\text{Porosity} = \frac{\rho_{ct} - \rho_{cm}}{\rho_{ct}} \times 100 \tag{4}$$

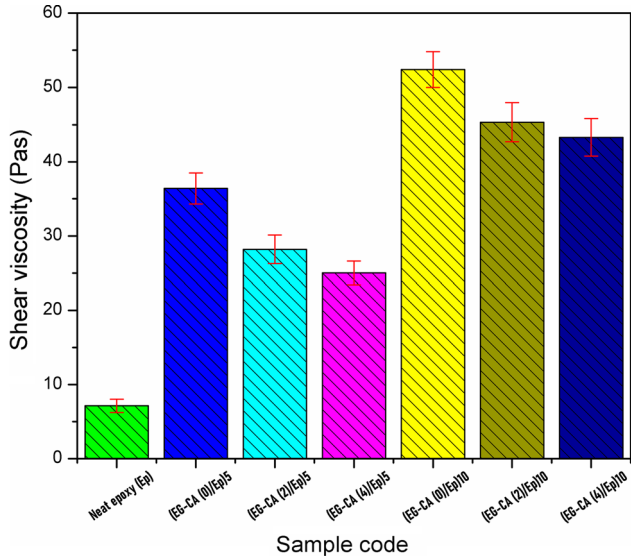

Fig. 9. Viscosity of neat epoxy and its EG-Cu-compound hybrid composite system.

The bulk density of EG and EG-Cu compound hybrid filler was measured using a graduated cylinder. As expected, the density of the epoxy composite system increased with the accumulation of EG-Cu-compound hybrid filler as documented in Table IV. The composite comprising only 10 wt.% EG, is showing lower density and higher porosity as compared to the composite containing only 5 wt.% of the same. This is due to the lower density of EG (0.033 g/cc) which reduced the bulk density of the composite. Moreover, the epoxy resin may not able to fill the entire void and air gaps of EG at the time of fabrication due to the viscosity rise and poor wettability of epoxy (Fig. 9). But after the addition of EG-Cu-compound hybrid filler, the density has been increased and porosity has been decreased as reported in Table IV.[56–58]

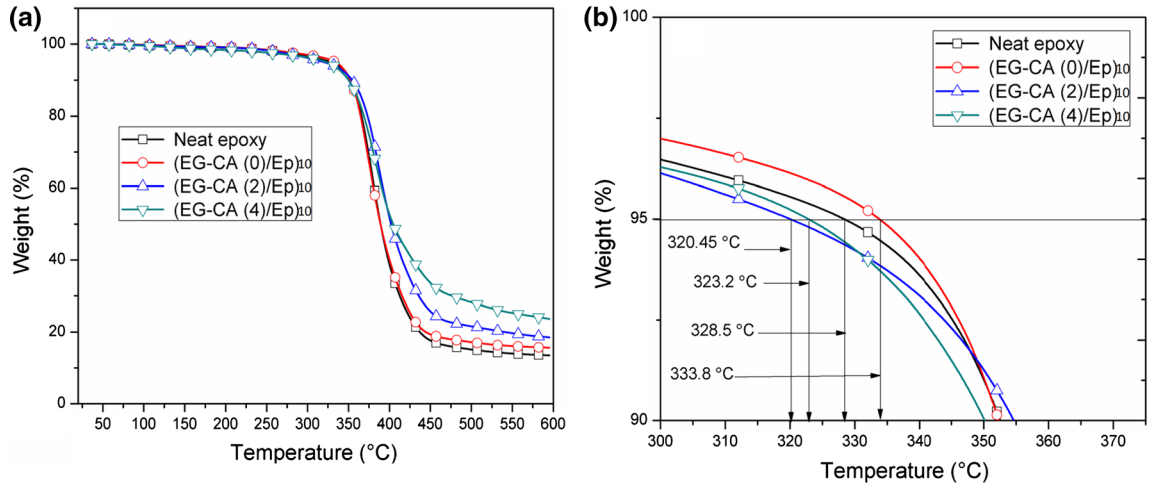

Fig. 10. TGA thermogram of (a) neat epoxy and EG-Cu-compound filler loaded hybrid composites at 10 wt.% with different ratio of CA mixing (b) at 5% wt loss.

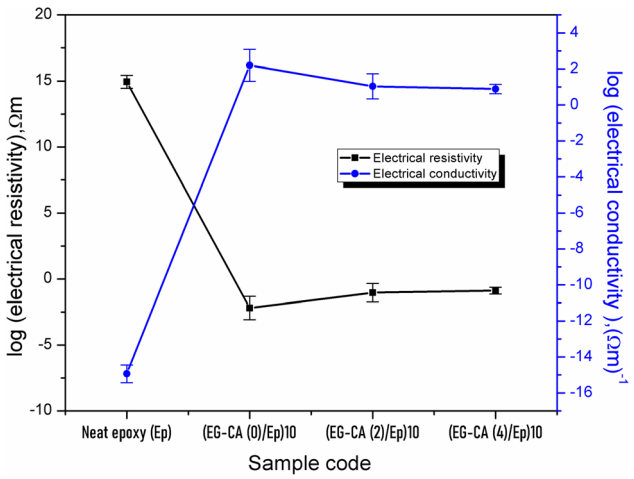

Fig. 11. Electrical conductivity and resistivity of EG/epoxy composite system.

To identify the processing condition of the developed epoxy composite, the rheological property such as shear viscosity before curing was analyzed. At shear rate 40 s^{-1}, the viscosity was measured at room temperature as depicted in Fig. 9. When 5 wt.% EG is added, the viscosity of (EG-CA (0)/Ep)5 designated composite showed a higher value than corresponding EG-Cu compound loaded hybrid composite. This is due to the force exerted by CA particles on the EG at the time of high-frequency mixing making the hybrid filler more compact than only EG. Similarly, at 10 wt.% of EG loading ((EG-CA (0)/Ep)10), the viscosity showed the highest value among all the designated composites. This may be due to the porous structure and very low density of EG which results in non-homogenous mixing inside the epoxy matrix. Also, filler restricts the chain mobility of the epoxy resin which develops the resistance of the flow in the composite. However, at the same wt.%, the EG-Cu compound loaded hybrid composite indicated the reduced value of viscosity. The diminished viscosity is due to the CA particle bombardment on EG surface causes the reduction in the graphitic layers gap leading to an increase in the density of hybrid fillers.[42]

The stability of pristine epoxy and epoxy hybrid composites at 10 wt.% loading was measured by TGA as shown in Fig. 10. Corresponding to 5% weight loss, the neat epoxy is stable up to 328.5°C and resin loaded with 10 wt.% of neat EG showed the decomposition temperature of 333.8°C. In this stage, there is some fluctuation observed in the degradation temperature of the composite as shown in Fig. 10b. The removal of moisture and the decomposition of oligomers are the reasons behind the fluctuation in degradation temperature at 5% wt loss.[21,59]

At 50% weight loss, the thermal degradation temperature of neat epoxy is 386°C and composite filled with 10 wt.% of EG showed 387°C. The composite entitled as (EG-CA (2)/Ep)10 and (EG-CA (4)/Ep)10 demonstrated the decomposition temperature of 404°C and 407°C, respectively. Due to the porous structure of EG inside the matrix, it absorbs heat, for which the actual decomposition starts at a higher temperature. Also, the barrier effect of fillers improves the resistance to thermal degradation and prevents the diffusion of disintegration yield from the polymer into the gas phase.[21] When EG-Cu-compound hybrid filler with the same weight % taken into consideration, the decomposition temperature takes little advantage due to the presence of Cu and Cu oxide (s) nanoparticles. From this analysis, it is obvious that the presence of Cu-compound nanoparticles contributes to the improvement of the degradation temperature. This is due to the better compatibility and interaction of Cu-compound nanoparticles with EG inside the epoxy resin and also Cu nanoparticles acting as a catalyst in the matrix for the heat flow as the thermal

conductivity of copper is ~ 400 W/mK. Both thermal stability and residual mass retention in case of EG-Cu-compound filled epoxy composite displayed better results as compared to simply EG loaded epoxy composite. However, the above described hybrid epoxy composite performed better below 280°C and a negligible weight loss was noticed at this temperature range. Hence, this developed hybrid epoxy composite containing EG-Cu-compound as a hybrid filler is possibly better suitable as interface material for high heat-generating electronic components.

The log of electrical resistivity and conductivity of an optimized epoxy composites system containing 10 wt.% of EG and EG-Cu compound hybrid filler is shown in Fig. 11. It is observed that composite coded as (EG-CA (0)/Ep)10 (10 wt.% of EG), revealed the sudden decrease in electrical resistivity value from as compared to the electrical resistivity of epoxy resin and consequently, electrical conductivity increased. It is pragmatic to relate the percolation theory for the understanding of the EG/epoxy composite system. According to the percolation concept, EG inside the epoxy matrix formed a cluster that further leads to the formation group of the cluster by creating 3-D electron conductivity networks. This is possible when filler addition reached percolation threshold limit.[60] Near the percolation threshold, there must be a decrease in electrical resistivity which is also called a percolation transition point.

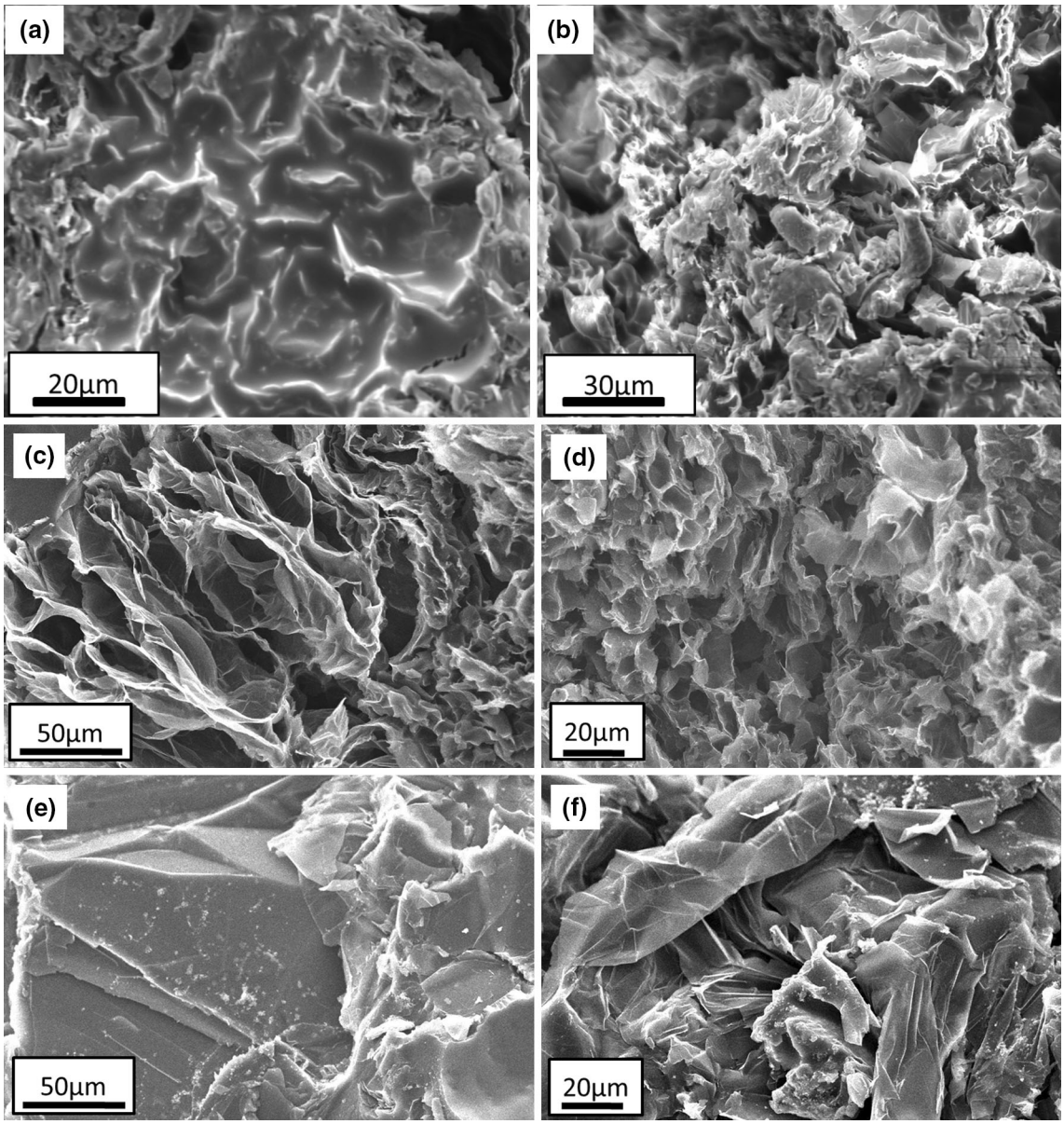

Fig. 12. SEM images of epoxy composite system (a) and (b) at 5 wt.% EG loaded, (c, d) 10 wt.% EG loaded, (e, f) at 10 wt.% of EG-Cu-compound loaded (EG:CA = 5:4).

Further incorporation of Cu compound coated EG hybrid filler, the electrical resistivity slightly increased as compared to bare EG loaded composite. This is due to the combined effect of Cu, CuO and Cu_2O nanoparticles on the EG surface. The Cu possesses high electrical conductivity of 6×10^7 $(\Omega\ m)^{-1}$ whereas CuO and Cu_2O are ceramic material exhibit very low electrical conductivity. It is known that Cu_2O is metal deficient semiconductor that contains a stoichiometric excess of oxygen.[61] The bandgap energy which distinguishes the insulative, semi-conductive and conductive property of various material is also used to define the electron transform property of copper(I) oxide (Cu_2O) and copper(II) oxide (CuO). The bandgap or forbidden gap energy of Cu_2O ranges from 2.1 eV to 2.6 eV, however, CuO shows 1.3 eV to 2.1 eV which defines the electron conduction between valance band and conduction band.[61] Hence, the copper(I) oxide (cuprous oxide) displays higher electrical resistance than copper(II) oxide (cupric oxide).[62,63]

The SEM images of Fig. 12a and b represent the fracture surface of 5 wt.% EG loaded epoxy composite. The graphite network inside the matrix is well observed which is attributed to that the formation of 3-D conducting networks inside the epoxy matrix. Due to the low filler fraction of EG, the dispersion of filler inside the matrix is well balanced with minimizing hole and pore. The impregnation of the epoxy resin inside the EG layer is better as compared to 10 wt.% loaded EG/epoxy composite as shown in Fig. 12c and d. Due to poor wettability of epoxy over EG, the introduction of micro-holes and air gaps lead to the reduction of thermal and mechanical properties as air contributes no TC and mechanical strength. But due to the presence of an air gap between graphitic layers, the electrical insulating properties remain with a specified range. SEM image of 10 wt.% incorporated EG-Cu compound hybrid filler with epoxy as described in Fig. 12c and d. The incorporation of Cu-compound nanoparticles with EG, the nanoparticles enter the gap of EG layers and stacks which reduce the air-trapping capacity and make defect-free dispersion inside the matrix, leads to high TC as well as high thermal stability.[10,21,64]

CONCLUSION

In this study, a novel hybrid of EG-Cu-compound was synthesized and applied to epoxy resin for TIMs preparation. The morphology analysis through XRD, SEM, and TEM confirmed the formation of Cu-compound nanoparticles of graphene layers of EG. The number and quantity of nanoparticles decorated and the physical process of thermal filler loading is complicated. The TC of 10 wt.% EG-Cu-compound (EG: CA::5:4) loaded hybrid composite demonstrated 1081.34% enhancement as compared to neat epoxy. The TC and thermal stability at 10 wt.% loading of thermal filler are quite praiseworthy to make light and multifunctional TIMs. The lap shear strength of 5 and 10 wt.% added EG-Cu compound hybrid (EG: CA::5:4) was better than only EG added corresponding epoxy composite. The viscosity and porosity evaluation restricted the loading of the filler system to 10 wt.%. The electrical conductivity of 10 wt.% filled epoxy composite reached to the semiconducting range of electron transportation. The results obtained from the above discussion throughout the article make it promising to develop high-efficient, multifunctional TIMs for thermal management of advanced electronics and optoelectronic devices.

ACKNOWLEDGMENTS

This work is supported by the Board of Research Board in Nuclear Science (BRNS), Department of Atomic Energy (DAE), Govt. of India (Project No. 39/14/01/2018-BRNS/39,001).

REFERENCES

1. S.K. Nayak, S. Mohanty, and S.K. Nayak, *SN Appl. Sci.* 1, 337 (2019).
2. M. Li, Y. Wan, Z. Gao, G. Xiong, X. Wang, C. Wan, and H. Luo, *Mater. Des.* 51, 257 (2013).
3. T.L. Li and S.L.C. Hsu, *J. Phy. Chem. B* 114, 6825 (2010).
4. M. Ponce, A.J. Martínez, J. Correa, M. Cotorogea, and J. Arau, *IEEE Trans Power Electr.* 21, 532 (2006).
5. F. Sarvar and D.C. Whalley, *J. Electron. Manuf.* 9, 269 (1999).
6. A.E. Bergles, *IEEE Trans. Compon Packag Manuf Technol* 26, 6 (2003).
7. C.C. Teng, C.C.M. Ma, C.H. Lu, S.Y. Yang, S.H. Lee, M.C. Hsiao, M.Y. Yen, K.C. Chiou, and T.M. Lee, *Carbon* 49, 5107 (2011).
8. W. Cui, F. Du, J. Zhao, W. Zhang, Y. Yang, X. Xie, and Y.W. Mai, *Carbon* 49, 495 (2011).
9. S.H. Song, K.H. Park, B.H. Kim, Y.W. Choi, G.H. Jun, D.J. Lee, B.S. Kong, K.W. Paik, and S. Jeon, *Adv. Mater.* 25, 732 (2013).
10. S.Y. Mun, H.M. Lim, and D.J. Lee, *Thermochim. Acta* 619, 16 (2015).
11. S. Choi, K. Kim, J. Nam, and S.E. Shim, *Carbon* 60, 254 (2013).
12. T.C. Mokhena, Mochane Mokhena, M.J. Mochane, J.S. Sefadi, S.V. Motloung, and D.M. Andala, *Impact Therm. Conduct. Energy Technol.* 6, 181 (2018).
13. C.P. Wong and R.S. Bollampally, *J. Appl. Polym. Sci.* 74, 3396 (1999).
14. L.E. Nielsen, *J. Appl. Polym. Sci.* 17, 3819 (1973).
15. Y.P. Mamunya, V.V. Davydenko, P. Pissis, and E.V. Lebedev, *Eur. Polym. J.* 38, 1887 (2002).
16. H. Yu, L. Li, and Y. Zhang, *Scr. Mater.* 66, 931 (2012).
17. Y. Lin, K.A. Watson, M.J. Fallbach, S. Ghose, J.G. Smith Jr, D.M. Delozier, W. Cao, R.E. Crooks, and J.W. Connell, *ACS Nano* 3, 871 (2009).
18. L.T. Drzal and H. Fukushima, *Polym. Prepr. (USA)* 42, 42 (2001).
19. V. Sridhar, J.H. Jeon, and I.K. Oh, *Carbon* 48, 2953 (2010).
20. X. Huang, Z. Yin, S. Wu, X. Qi, Q. He, Q. Zhang, Q. Yan, F. Boey, and H. Zhang, *Small* 7, 1876 (2011).
21. Z. Wang, R. Qi, J. Wang, and S. Qi, *Ceram. Int.* 41, 13541 (2015).
22. P.A. Khomyakov, G. Giovannetti, P.C. Rusu, G.V. Brocks, J. Van den Brink, and P.J. Kelly, *Phys. Rev. B* 79, 195425 (2009).
23. Q.J. Wang and J.G. Che, *Phys. Rev. Lett.* 103, 066802 (2009).
24. Z. Lin, D. Han, and S. Li, *J. Therm. Anal. Calorim.* 107, 471 (2012).

25. M. Afzal, P. Butt, and H. Ahmad, *J. Therm. Anal. Calorim.* 37, 1015 (1991).
26. S.A.A. Mansour, *J. Therm. Anal. Calorim.* 46, 263 (1996).
27. K. Zhang, J. Hong, G. Cao, D. Zhan, Y. Tao, and C. Cong, *Thermochim. Acta* 437, 145 (2005).
28. E. Neubauer, G. Korb, C. Eisenmenger-Sittner, H. Bangert, S. Chotikaprakhan, D. Dietzel, A.M. Mansanares, and B.K. Bein, *Thin Solid Films* 433, 160 (2003).
29. X.Y. Yan, X.L. Tong, Y.F. Zhang, X.D. Han, Y.Y. Wang, G.Q. Jin, Y. Qin, and X.Y. Guo, *Chem. Commun.* 48, 1892 (2012).
30. M. d'Halluin, T. Mabit, N. Fairley, V. Fernandez, M.B. Gawande, E. Le Grognec, and F.X. Felpin, *Carbon* 93, 974 (2015).
31. L. Chen, P. Zhao, H. Xie, and W. Yu, *Compos. Sci. Technol.* 125, 17 (2016).
32. M. Liu, M.C. Lin, and C. Wang, *Nanoscale Res. Lett.* 6, 297 (2011).
33. S.Y. Mun, H.M. Lim, and S.H. Lee, *Mater. Res. Bull.* 97, 19 (2018).
34. E.T. Swartz and R.O. Pohl, *Appl. Phys. Lett.* 51, 2200 (1987).
35. A. Malas, C.K. Das, A. Das, and G. Heinrich, *Mater. Des.* 39, 410 (2012).
36. B. Debelak and K. Lafdi, *Carbon* 45, 1727 (2007).
37. M. Raffi, S. Mehrwan, T.M. Bhatti, J.I. Akhter, A. Hameed, W. Yawar, and M.M. ulHasan, *Ann. Microbiol.* 60, 75 (2010).
38. T.T. Baby, S.J. Aravind, T. Arockiadoss, R.B. Rakhi, and S. Ramaprabhu, *Sens. Actuat. B Chem.* 145, 71 (2010).
39. I.V. Lightcap, T.H. Kosel, and P.V. Kamat, *Nano Lett.* 10, 577 (2010).
40. S.E. Gwaily, G.M. Nasr, M.M. Badawy, and H.H. Hassan, *Polym. Degrad. Stabil.* 47, 391 (1995).
41. K.M. Shahil and A.A. Balandin, *Nano Lett.* 12, 861 (2012).
42. R. Kumar, S. Mohanty, S.K. Nayak, and S.N. Appl, *Sci.* 1, 180 (2019).
43. A.A. Balandin, *Nat. Mater.* 10, 569 (2011).
44. M.T. Pettes, H. Ji, R.S. Ruoff, and L. Shi, *Nano Lett.* 12, 2959 (2012).
45. H. Fang, Y. Zhao, Y. Zhang, Y. Ren, and S.L. Bai, *ACS Appl. Mater. Interfaces* 9, 26447 (2017).
46. H. Fang, X. Zhang, Y. Zhao, and S.L. Bai, *Compos. Sci. Technol.* 152, 243 (2017).
47. H.S. Kim, H.S. Bae, J. Yu, and S.Y. Kim, *Sci. Rep.* 6, 26825 (2016).
48. H. Jung, S. Yu, N.S. Bae, S.M. Cho, R.H. Kim, S.H. Cho, I. Hwang, B. Jeong, J. Hwang, and S.M. Hong, *ACS Appl. Mater. Interfaces* 7, 15256 (2015).
49. P.K. Ghosh, S. Halder, M.S. Goyat, and G. Karthik, *J. Adhes.* 89, 55 (2013).
50. R. Kumar, S.K. Nayak, S. Sahoo, B.P. Panda, S. Mohanty, and S.K. Nayak, *J. Mater. Sci. Mater. El.* 29, 16932 (2018).
51. R. Sun, H. Yao, H.B. Zhang, Y. Li, Y.W. Mai, and Z.Z. Yu, *Compos. Sci. Technol.* 137, 16 (2016).
52. R. Aradhana, S. Mohanty, and S.K. Nayak, *Compos. Sci. Technol.* 169, 86 (2019).
53. A.G. Evans, *Philos. Mag.* 26, 1327 (1972).
54. D.J. Green, P.S. Nicholson, and J.D. Embury, *J. Mater. Sci.* 14, 1413 (1979).
55. P.K. Ghosh and M. Balaram, *Trans. Indian Inst. Metals* 58, 115 (2005).
56. Y. Hwang, M. Kim, and J. Kim, *Chem. Eng. Trans.* 246, 229 (2014).
57. S.L. Chung and J.S. Lin, *Molecules* 21, 670 (2016).
58. I.M. Afanasov, D.V. Savchenko, S.G. Ionov, D.A. Rusakov, A.N. Seleznev, and V.V. Avdeev, *Inorg. Mater.* 45, 486 (2009).
59. S. Ibrahim and M.R. Johan, *Int J ElectrochemSci* 7, 2596 (2012).
60. L. Melnyk, *Technol. Audit Prod. Reserv.* 3, 28 (2017).
61. A.A. Ogwu, T.H. Darma, and E. Bouquerel, *J. Achiev. Mater. Manuf. Eng.* 24, 172 (2007).
62. R. Padiyath, J. Seth, and S.V. Babu, *Thin Solid Films* 239, 8 (1994).
63. V.F. Drobny and L. Pulfrey, *Thin Solid Films* 61, 89 (1979).
64. A. Yasmin, J.J. Luo, and I.M. Daniel, *Compos Sci Technol* 66, 1182 (2006).